J Appl Electrochem (2010) 40:133–141
DOI 10.1007/s10800-009-9989-9

ORIGINAL PAPER

Fabrication of manganese oxide electrodes by radio frequency sputtering for electrochemical capacitors

Chuen-Chang Lin · Chih-Chung Lee

Received: 21 March 2009 / Accepted: 16 August 2009 / Published online: 28 August 2009
© Springer Science+Business Media B.V. 2009

Abstract Manganese oxide thin films were sputtered on graphite foils by radio frequency (RF) sputtering. At the 1,000th cycle of potential cycling, maximum mass specific capacitance of 341 F g^{-1} was obtained in 0.5 M LiCl and with optimum sputtering conditions (5 sccm of oxygen, 20 mTorr, and 70 W) as well as annealing temperature (150 °C). These show its high electrochemical stability and good mass specific capacitance at a higher sweep rate of 100 mV s^{-1}. In addition, the higher the volume flow rates of oxygen, the larger the amount of trivalent manganese oxide and the higher the surface roughness, the higher the mass specific capacitance at lower volume flow rates of oxygen, but the amounts of trivalent manganese oxide were almost the same and the mass specific capacitance decreased due to decreasing surface roughness at higher volume flow rates of oxygen. Furthermore, the geometric specific capacitance increases with increasing sputtering pressure and power.

Keywords Sputtering · Manganese oxide · Surface roughness · Annealing · Electrochemical capacitors

1 Introduction

Electrochemical capacitors are charge-storage devices, which possess a higher power density and a longer cycle life than batteries [1–3]. Their applications include stop/go power sources for hybrid vehicles, starting power for fuel cells, and burst-power generation in electronic devices, etc. [4–9]. Electrochemical capacitors are classified into two types, electric double layer capacitors (EDLC) and pseudo-capacitors according to their energy-storage mechanisms. The capacitance of an EDLC arises from the separation of charge at the interface between the electrolyte and the electrode with a high surface area inert material such as activated carbon [9, 10]. By contrast, pseudo-capacitance arises from fast and reversible redox reactions of electro-active materials with several oxidation states [1, 9–15].

Amorphous hydrous ruthenium oxide prepared by the sol–gel method and annealed at low temperature (<150 °C) has been found to possess very high mass specific pseudo-capacitance value of 720 F g^{-1} at 2 mV s^{-1} [16, 17] and the symmetry of cyclic voltammetry (CV) curves improved significantly at high voltage scan rates [18]. However, ruthenium is not suitable for wider commercialization due to being relatively expensive. Hence, the more economical manganese oxide with a variety of stable Mn valence states appears to be a substitutive electrode material for electrochemical capacitors. Therefore, manganese oxides were prepared by different wet processes (anodic deposition, sol–gel, and co-precipitation) for their application as electrode materials in electrochemical capacitors [3, 10, 19–21]. The stability of the amorphous hydrous manganese oxide anodically deposited from the $MnSO_4$ solutions at various pHs has been enhanced by an annealing treatment, albeit capacitance gradually decreased with increasing annealing temperature [19]. Hydrous manganese oxide deposited on a carbon substrate at anodic potentials of 0.5 V_{SCE} in 0.25 M manganese acetate solution at 25 °C exhibited maximum mass specific capacitance of 240 F g^{-1} in 2 M KCl solution at a potential scan rate of 5 mV s^{-1}. The higher the deposition potential, the lower the mass specific capacitance achieved because of lower porosity and a smaller amount of

C.-C. Lin (✉) · C.-C. Lee
Department of Chemical and Materials Engineering, National Yunlin University of Science and Technology, 123 University Road, Sec. 3, Douliu, Yunlin 64002, Taiwan
e-mail: linchuen@yuntech.edu.tw

trivalent manganese oxide [3]. A thin film of amorphous hydrous manganese oxide prepared by the dip-coated sol–gel derived technique involving $KMnO_4$ and $MnCl_2$ was found to exhibit a high mass specific capacitance of 698 F g^{-1} (at a scan rate of 5 mV s^{-1} and in 0.1 M Na_2SO_4) and long cycle life. However, the discharge time achieved was only about 1.1 s at constant current of 0.1 mA and the slope of the constant current discharge curve was not exactly constant [20]. In addition, manganese oxide was prepared at different pH and temperatures, then precipitated into activated carbon by the chemical impregnation method, and finally annealed in nitrogen gas at different temperatures. Maximum capacitance of 461.3 F g^{-1} was obtained in a 0.1 M Na_2SO_4 solution for manganese oxide prepared under the better/superior conditions (pH = 13.11 and $T = 25$ °C) and annealed at a temperature of 195 °C [21]. Moreover, manganese oxide was coated on a graphite electrode by immersion. Durations for immersion were varied to control the amount of manganese oxide coated onto the electrode surface. Maximum capacitance of 556 mF cm^{-2} was obtained in 0.5 M LiCl and with better/superior conditions (immersion time = 80 min and potential scan rate = 10 mV s^{-1}) [22]. However, some residual impurities could be carried over from these wet processes, and these might affect electrochemical properties (such as conductance) of electrodes. Thus, dry processes such as sputtering were applied to fabricate manganese oxides in this research. Mn films were deposited by sputtering and then manganese oxide films were synthesized by anodic oxidation; the mass specific capacitance of the films yielded 400–450 F g^{-1} at a potential scan rate of 5 mV s^{-1} [9]. A ruthenium oxide thin film was deposited on a Pt/Ti/Si substrate by a specially designed direct current (DC) reactive sputtering method: the capacitance per volume of the thin film supercapacitor (TFSC) at the first cycle was 38 mF cm^{-2} μm^{-1} [23].

Meanwhile contamination, the physical properties (such as surface roughness) of the substrate, film thickness, and some sputtering parameters (such as sputtering pressure, substrate temperature, and bias voltage), etc., have an effect on adhesion [24–29], which influences operational stability of electrochemical capacitors. In addition, ruthenium oxide films were deposited on Si and Ti substrates by reactive radio frequency (RF) magnetron sputtering and the total anodic voltammetric charges increased with increasing roughness factor [30]. Since the highly rough surface should possess the high surface area, the mass specific capacitance also increased with increasing the roughness factor for manganese oxide [31]. Furthermore, the sputtering yield is reduced so that the deposition rate is also reduced when the oxygen concentration in the sputtering gas (argon and oxygen) is increased, because metal–oxygen reaction occurs on the target surface [32] and the molecular weight of argon is larger than that of oxygen. Thus, the oxygen concentration changes the surface roughness, crystallization, and oxidation state, which influence specific capacitance and operational stability of electrochemical capacitors. Moreover, sputtering also offers the opportunity to control structural (such as surface roughness and crystallization) and stoichiometric (oxidation state) development of mixing metal–oxygen materials.

Manganese oxide prepared by anodic deposition and annealed at or above 500 °C has been found to form crystalline, decrease the Mn–OH (hydroxide) as well as the H–O–H (water), and increase the Mn–O–Mn (oxide oxygen) compared with below 500 °C—annealed and as-deposited [33]. The electrochemical activity of $MnNi_{0.25}O_x$ decreases at high annealing temperature because of separation of the active material into crystalline phases by diffusion and then its mass specific capacitance decreases [34]. Therefore, a simpler one-step RF magnetron sputtering dry process for depositing manganese oxide onto the surface of a graphite foil electrode was applied to seek maximum specific capacitance at optimum conditions in this study. Subsequently, the surface morphology, mean roughness, and chemical environment of the graphite foil electrode were examined by field emission scanning electron microscope (FE-SEM), atomic force microscope (AFM), and X-ray photoelectron spectroscopy (XPS).

2 Experimental methods

A graphite foil was used as a substrate due to its lower specific resistance (6.3–7.3, lower than that of activated carbon and silicon) [35]. The graphite foil (1 × 1 or 1 × 2 cm^2) was abraded with SiC paper and then rinsed ultrasonically with de-ionized water for 10 min. It was then etched in 6 M aqueous HCl at room temperature for 30 min and subsequently rinsed ultrasonically with de-ionized water for 10 min. Next, it was degreased ultrasonically in acetone until any surface grease was completely eliminated. Finally, it was rinsed with pure de-ionized water, subsequently oven-dried in air (50 °C) to constant weight, and then reweighed for sputtering.

The manganese oxide film was deposited on the pretreated and grounded graphite foil substrate by reactive RF magnetron sputtering from a 3-inch disk Mn oxide (MnO_2, purity: 99.9%, purchased from SCM, INC) target in a vacuum chamber with a background pressure of 7×10^{-6} Torr. The distance between the target and the substrate was 6 cm. During deposition, the substrate was not intentionally heated. The sputtering time and the volume flow rate of argon were maintained at 60 min and 25 sccm, respectively. The volume flow rates (2.5, 5, and 7.5 sccm) of oxygen, sputtering pressure (10, 20, and 30 mTorr), and

power (50, 70, and 80 W) were varied. Next, the graphite foils with manganese oxide thin films were weighed and thus the mass of manganese oxide could be determined. Finally, the manganese oxide thin films were annealed in air for 90 min at various temperatures (150 and 300 °C) under a temperature increment rate of 10 °C min^{-1}.

Electrochemical measurements for the prepared graphite foil electrodes were performed by an electrochemical analyzer (CH Instruments CHI 608B, USA). The three-electrode cell consisted of Ag/AgCl as the reference electrode, Pt as the counter electrode and the prepared electrode as the working electrode. The electrolytes were degassed with purified nitrogen gas before voltammetric measurements, and nitrogen was passed over the solution during all the measurements. The solution temperature was maintained at 25 °C by means of a circulating water thermostat (HAAKE DC3 and K20, Germany). The CV was taken with a potential scan rate of 100 mV/s (at a sweep rate lower than 100 mV/s, its CV does not show the rectangular and symmetric current-potential characteristics of a capacitor) and 0.5 M aqueous electrolyte (LiCl, pH = 6.7). The potential window in the range of 0–1 V was used in all measurements except where stated. Capacitance is normalized to 1 g of manganese oxide. However, focusing only on the mass specific capacitance in the electrode material evaluation of electrochemical capacitors can be misleading in terms of practical applications since capacitance also depends on kinetics and may not simply increase linearly with increasing material mass after the thickness of the not well-structured porous material has reached the kinetic restriction on ion transfer in charge–discharge processes [36]. Therefore, the practically accessible capacitance over a unit geometric area is also utilized in this research.

Surface morphology of the electrode prepared at different conditions was conducted by FE-SEM (JEOL JSM-6700F, Japan). Furthermore, the chemical environment of the electrode prepared at different volume flow rates of oxygen was explored by XPS (Fison VG. ESCA210, England). Additional information on the surface roughness of the electrodes prepared at different conditions was obtained by AFM (Digital Instrument NanoMan NS4 + D3100, USA).

3 Results and discussion

Cyclic voltammograms at a potential scan rate of 100 mV s^{-1} for the manganese oxide electrode (using optimum sputtering conditions: 5 sccm oxygen, 20 mTorr, and 70 W) without annealing are shown in Fig. 1, which shows a mirror image with respect to the zero-current line and a rapid current response on voltage reversal at potentials near the two limits of the potential window. These features indicate that

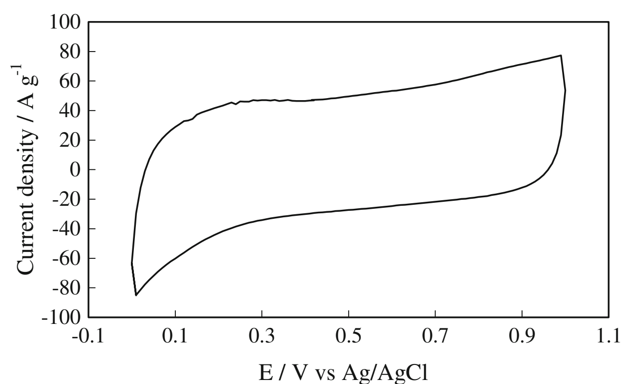

Fig. 1 Cyclic voltammograms (the 5th charge–discharge cycle) at a potential scan rate of 100 mV s^{-1} for the electrode (using optimum sputtering conditions: 5 sccm oxygen, 20 mTorr, and 70 W) without annealing

hydrated cations (such as Li^+ and proton) of the electrolyte (pH = 6.7) have a rapid chemisorption/desorption reaction rate and are involved in the charge-storage process within the very near surface thin layer of manganese oxide electrodes [37, 38].

Figure 2a shows the effects of sputtering pressure on the mass specific capacitance and depositing weight (using optimum sputtering conditions: 5 sccm oxygen and 70 W without annealing). The depositing weight increased with increasing sputtering pressure since the higher the sputtering pressure, the larger the amount of argon (25 sccm of argon > 5 sccm of oxygen) ions bombarding the target, and the higher the depositing rate, thus leading to increase depositing weight. The mass specific capacitance reached a maximum at 20 mTorr of sputtering pressure. The mass specific capacitance increased at the range from 10 to 20 mTorr of sputtering pressure. The reason behind this behavior may be explained as follows. Higher sputtering pressure (i.e., higher ion density and reflected neutral density) leads to higher collision frequencies and lower kinetic energy. The lower the kinetic energy, the lower the mobility on the surface of the substrate for particles (ions and reflected neutrals), and the higher the surface roughness (see Fig. 3, i.e., there is an increase in the height of the surviving particles in a particle-migration coalescence process), thus leading to higher mass specific capacitance (a similar result has been published in previous literature [30, 31]). However, mass specific capacitance declined at sputtering pressure in the range 20–30 mTorr. This picture may be attributed to a too high sputtering pressure, leading to too many ions as well as reflected neutrals, and thus causing a shadowing effect which enhances lots of collision probability, and so declining lots of kinetic energy/migration on the surface of the substrate for particles. This leads to a poorly packed structure (increase in larger porosities: see Fig. 4), and finally decreases surface roughness (see Fig. 3) and mass specific capacitance.

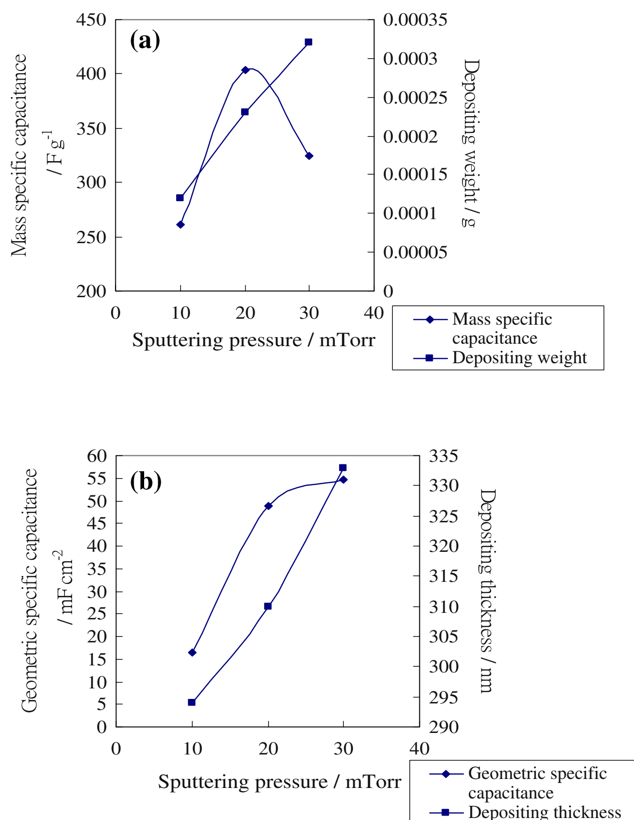

Fig. 2 The effects of sputtering pressure on **a** the mass specific capacitance and depositing weight, and **b** the geometric specific capacitance and depositing thickness (using optimum sputtering conditions: 5 sccm oxygen and 70 W without annealing)

Furthermore, Fig. 2b shows the effects of sputtering pressure on the geometric specific capacitance and depositing thickness. The depositing thickness increased with increasing sputtering pressure because the higher the sputtering pressure, the larger the amount of argon (25 sccm of argon > 5 sccm of oxygen) ions bombarding the target, and the higher the depositing rate, thus leading to increase depositing thickness. The geometric specific capacitance increased with increasing sputtering pressure. The reason behind this behavior may be that the higher the sputtering pressure, the more the amount as well as thicker of deposited manganese oxide (see Fig. 2a, b), and the more numerous the potentially electroactive sites, thus leading to higher geometric specific capacitance.

Figure 5a shows the effects of sputtering power on the mass specific capacitance and depositing weight (using optimum sputtering conditions: 5 sccm oxygen and 20 mTorr without annealing). The depositing weight increased with increasing sputtering power since the higher the sputtering power, the higher the depositing rate, and thus leading to increase depositing weight. The mass specific capacitance reached a maximum at 70 W. The mass specific capacitance increased at sputtering power in the range 50–70 W. This

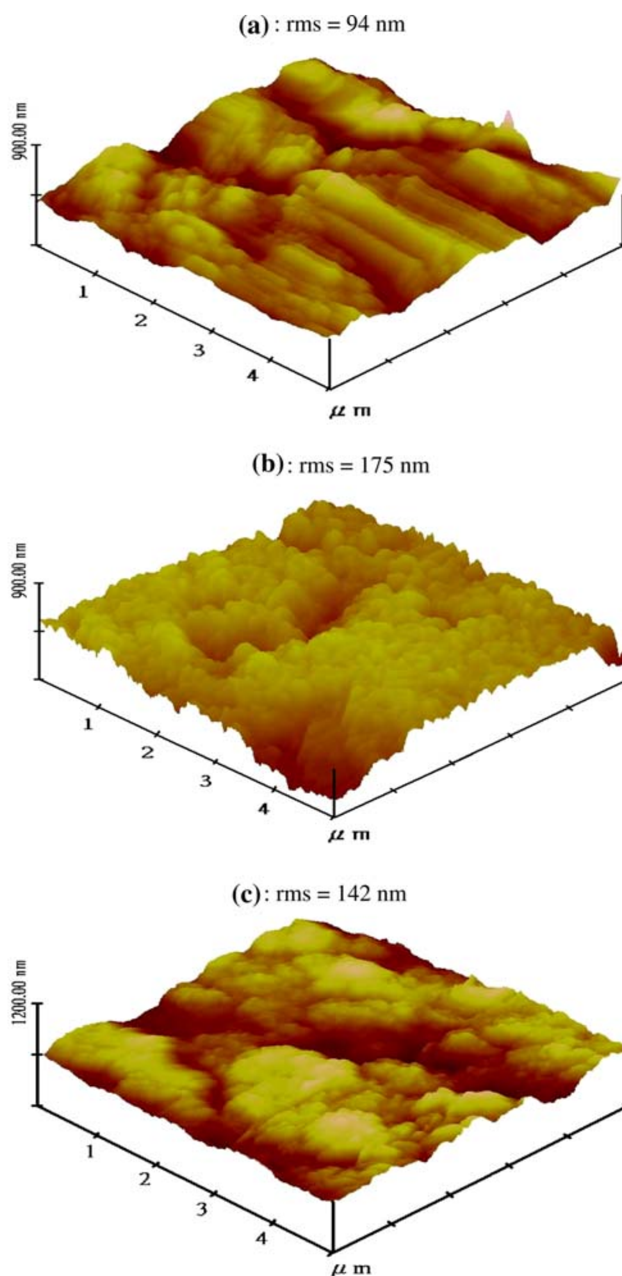

Fig. 3 AFM micrograph (**a** 10 mTorr, **b** 20 mTorr, and **c** 30 mTorr) of the electrode prepared at different pressure (using optimum sputtering conditions: 5 sccm oxygen and 70 W without annealing)

illustrates that the higher the sputtering power, the higher the sputtering yield, thus enhancing the deposition rate. Then the ions and reflected neutrals falling on the substrate have not enough time to rearrange and re-sputter, which leads to increasing surface roughness (see Fig. 6), and so leading to higher mass specific capacitance. However, the mass specific capacitance declined with sputtering power in the range 70–80 W. The reason behind this behavior may be attributed to a too high sputtering power, leading to a too strong ion as well as reflected neutral bombardment of the

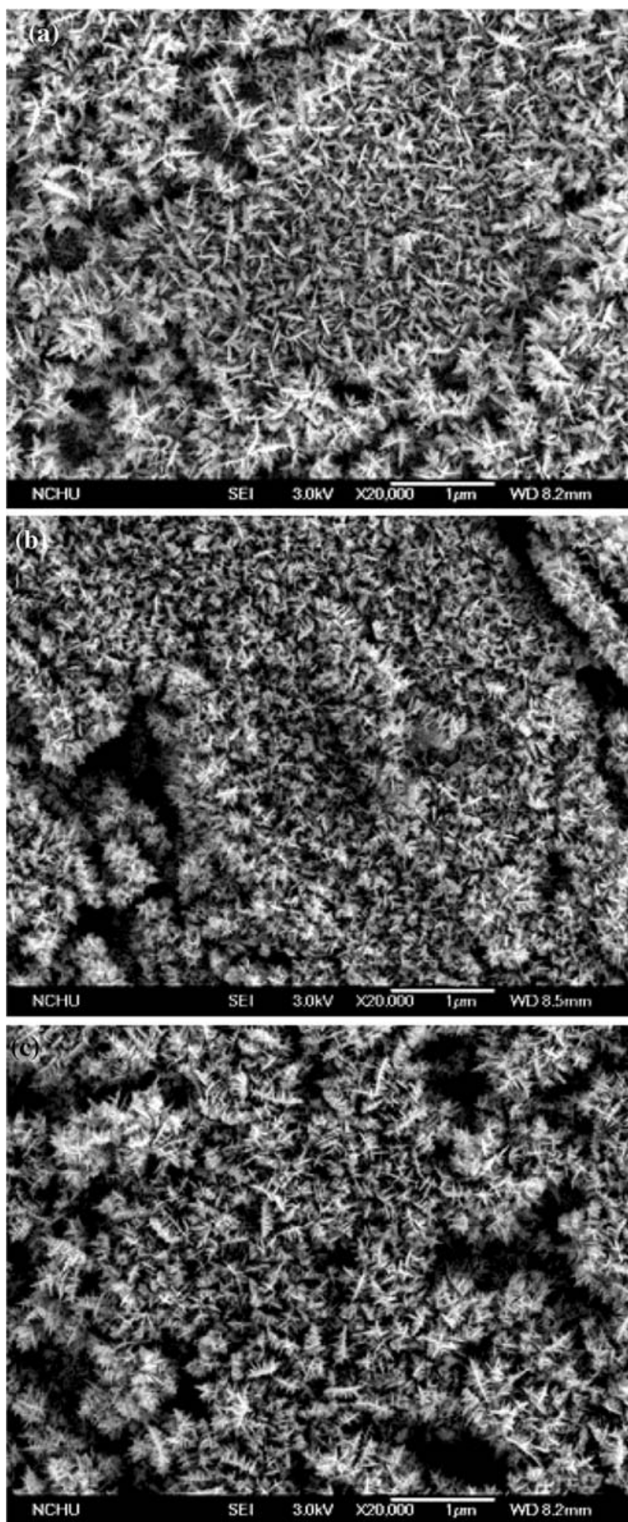

Fig. 4 SEM micrograph (**a** 10 mTorr, **b** 20 mTorr, and **c** 30 mTorr) of the electrode prepared at different pressure (using optimum sputtering conditions: 5 sccm oxygen and 70 W without annealing)

substrate surface, then only causing more damages, and thus decreasing surface roughness (see Fig. 6) and mass specific capacitance. Furthermore, Fig. 5b shows the effects of

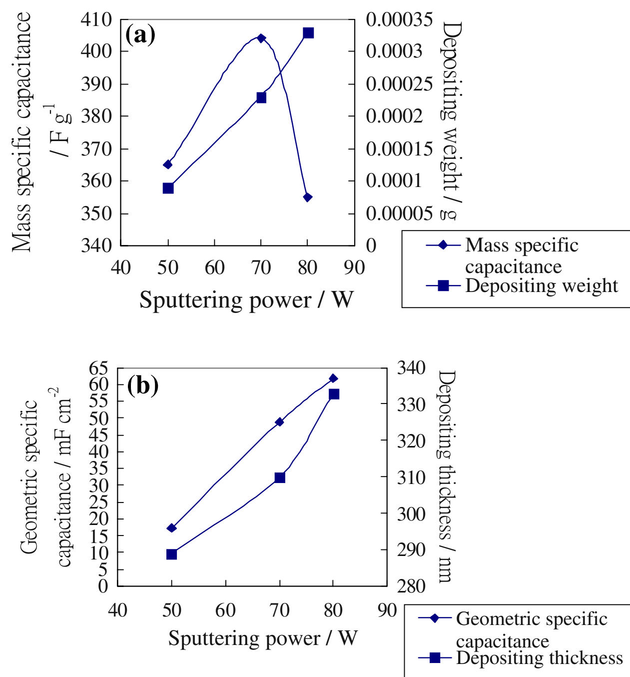

Fig. 5 The effects of sputtering power on **a** the mass specific capacitance and depositing weight, and **b** the geometric specific capacitance and depositing thickness (using optimum sputtering conditions: 5 sccm oxygen and 20 mTorr without annealing)

sputtering power on the geometric specific capacitance and depositing thickness. The depositing thickness increased with increasing sputtering power because the higher the sputtering power, the higher the depositing rate, and thus leading to increase depositing thickness. The geometric specific capacitance increased with increasing sputtering power. The reason behind this behavior may be that the higher the sputtering power, the more the amount as well as thicker of deposited manganese oxide (see Fig. 5a, b), and the more numerous the potentially electroactive sites, thus leading to higher geometric specific capacitance.

Figure 7a shows effects of different volume flow rates of oxygen on the mass specific capacitance and depositing weight (using optimum sputtering conditions: 20 mTorr and 70 W without annealing). The depositing weight decreased with increasing volume flow rates of oxygen since at higher volume flow rates of oxygen, the larger number of oxygen ions prevented argon ions from bombarding the target and even led to lighter oxygen ions (as opposed to heavier argon ions) bombarding the target. This would lead to a decrease the deposition rate and thus decrease depositing weight. The mass specific capacitance reached a maximum at 5 sccm oxygen. The mass specific capacitance increased in the range 2.5–5 sccm of oxygen. The reason behind this behavior may be that at higher volume flow rates of oxygen, the larger number of oxygen ions would lead to greater oxygen ion bombardment of the substrate surface because of a sheath voltage, enhancing

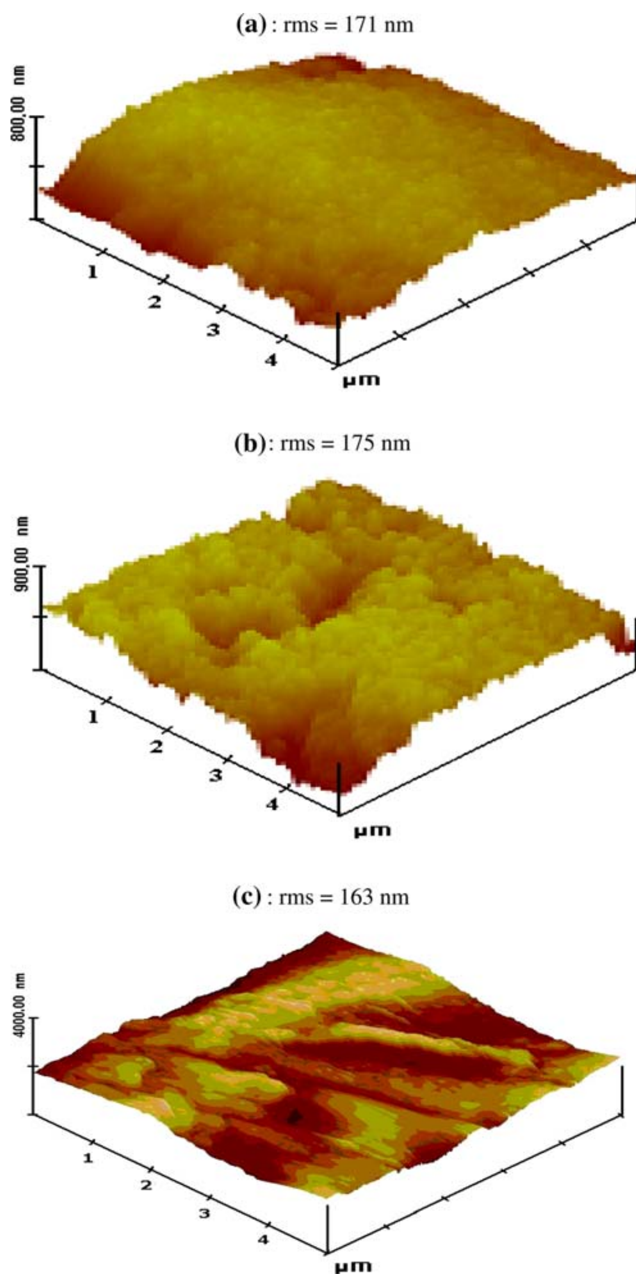

Fig. 6 AFM micrograph (**a** 50 W, **b** 70 W, and **c** 80 W) of the electrode prepared at different power (using optimum sputtering conditions: 5 sccm oxygen and 20 mTorr without annealing)

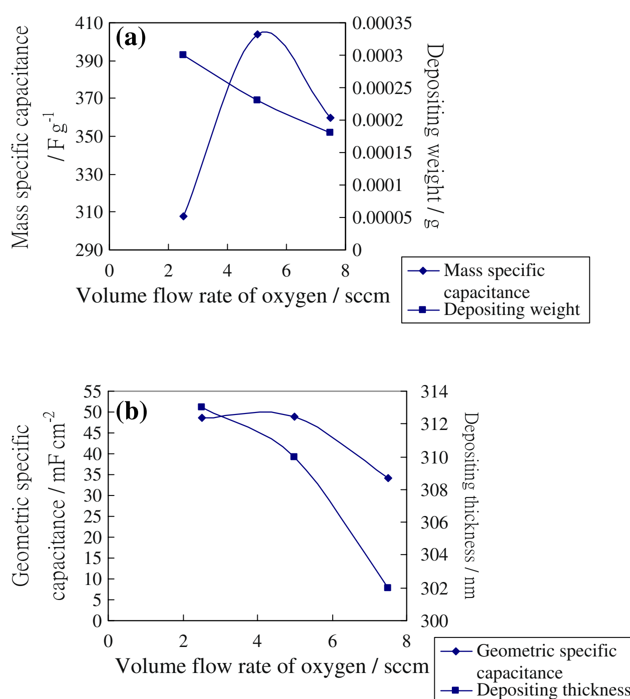

Fig. 7 The effects of different volume flow rates of oxygen on **a** the mass specific capacitance and depositing weight, and **b** the geometric specific capacitance and depositing thickness (using optimum sputtering conditions: 20 mTorr and 70 W without annealing)

surface roughness (see Fig. 8), and finally increasing mass specific capacitance. However, the mass specific capacitance declined in the range 5–7.5 sccm of oxygen. This may indicate that with too high a volume flow rate of oxygen, too many oxygen ions would cause a shadowing effect which prevented argon ions from bombarding the target and lead to lighter oxygen ions (as opposed to heavier argon ions) bombarding the target due to a sheath voltage. Thus, the sputtering yield is reduced so that the deposition rate drops. Consequently, ions falling on the substrate have sufficient time to rearrange themselves, which leads to decreasing surface roughness (see Fig. 8) and mass specific capacitance. In order to investigate the chemical environment of manganese oxide in the graphite foil electrode without annealing, XPS was used to examine the binding energy of manganese oxide thin films sputtered with optimum sputtering pressure (20 mTorr) as well as power (60 W) and different volume flow rates of oxygen. XPS spectral data of Mn $2p_{3/2}$, and Mn 3s for manganese oxide thin films sputtered with different volume flow rates of oxygen are listed in Table 1. The oxidation state of manganese oxide was determined by the differences in binding energies between the splitting peaks of Mn 3s in Table 1. The difference in binding energy for manganese oxide changed from 5.26 to 4.95 eV and 4.90 eV following 5 and 7.5 sccm oxygen, respectively. Thus, manganese oxide thin films sputtered with 2.5 sccm oxygen consist of Mn^{3+} as well as Mn^{4+} species and manganese oxide thin films sputtered with 5 or 7.5 sccm oxygen mainly consist of Mn^{4+} species [38, 39]. Therefore, at volume flow rates of oxygen in the range 2.5–5 sccm, the higher the volume flow rates of oxygen, the larger the amount of trivalent manganese oxide as well as the higher the surface roughness, and the higher the mass specific capacitance (see Table 1 and Figs. 7a, 8). A similar result has been published in previous literature [3, 30, 31]. However, at volume flow rates of oxygen in the range 5–7.5 sccm, the

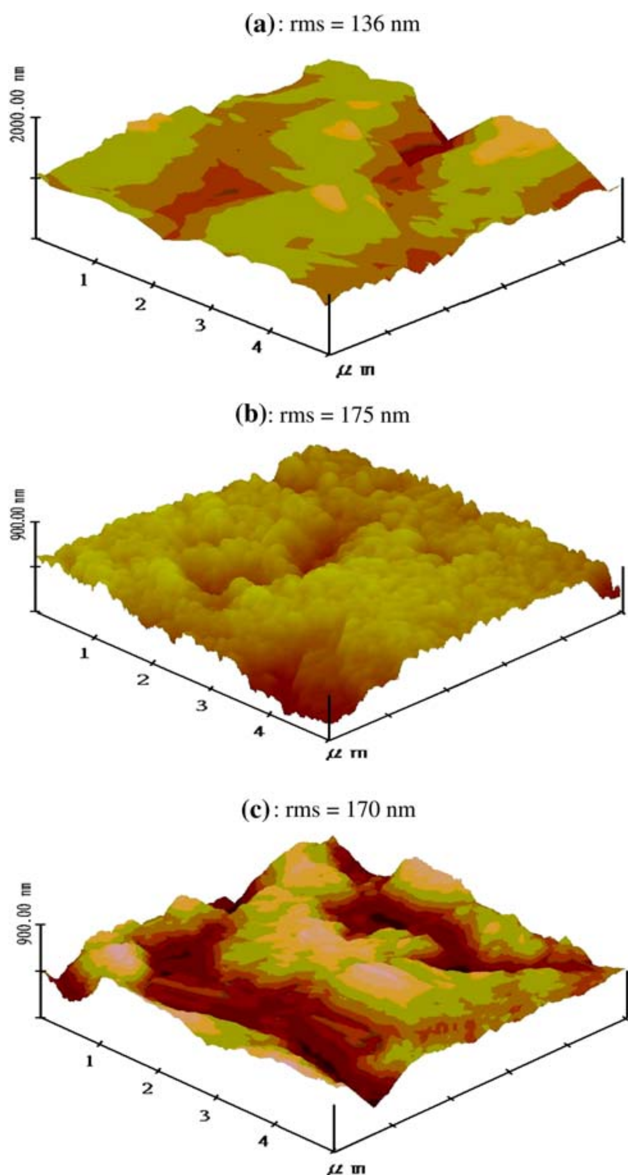

Fig. 8 AFM micrograph (**a** 2.5 sccm, **b** 5 sccm, and **c** 7.5 sccm) of the electrode prepared at different volume flow rates of oxygen (using optimum sputtering conditions: 20 mTorr and 70 W without annealing)

Table 1 XPS Mn $2p_{3/2}$ and Mn 3s binding energies (eV), bands, areas (%), and differences of binding energies (eV) for manganese oxide sputtered with optimum sputtering pressure (20 mTorr) as well as power (60 W) and different volume flow rates of oxygen

Sample	Mn $2p_{3/2}$	Mn 3s		
	Eb (eV)	Eb(1) (eV)	Eb(2) (eV)	$\triangle E$ (eV)
2.5 (sccm)	641.6	83.90	89.16	5.26
5 (sccm)	642.2	83.97	88.92	4.95
7.5 (sccm)	642.4	84.05	88.95	4.90

amounts of trivalent manganese oxide (or the valences of manganese) were almost the same due to excess oxygen and the mass specific capacitance decreased because of decreasing surface roughness (see Table 1 and Figs. 7a, 8). Furthermore, Fig. 7b shows the effects of different volume flow rates of oxygen on the geometric specific capacitance and depositing thickness. The depositing thickness decreased with increasing volume flow rates of oxygen because at higher volume flow rates of oxygen, the larger number of oxygen ions prevented argon ions from bombarding the target and even led to lighter oxygen ions (as opposed to heavier argon ions) bombarding the target. This would lead to a decrease the deposition rate and thus decrease depositing thickness. The geometric specific capacitance decreased with increasing volume flow rates of oxygen except 2.5 sccm oxygen. The reason behind this behavior may be that the higher the volume flow rate of oxygen, the less the amount as well as thinner of deposited manganese oxide (see Fig. 7a, b), and the less numerous the potentially electroactive sites, thus leading to lower geometric specific capacitance. However, manganese oxide thin films sputtered with 2.5 sccm oxygen do not mainly consist of Mn^{4+} species and thus lead to lower geometric specific capacitance.

Figure 9 shows the effects of different charge–discharge cycles and without annealing as well as with different annealing temperatures (150 and 300 °C) on the mass specific capacitance of the electrode (fabricated by optimum sputtering conditions: 5 sccm oxygen, 20 mTorr, and 70 W). At the 1,000th cycle of potential cycling, the electrode annealed at a temperature of 150 °C possessed

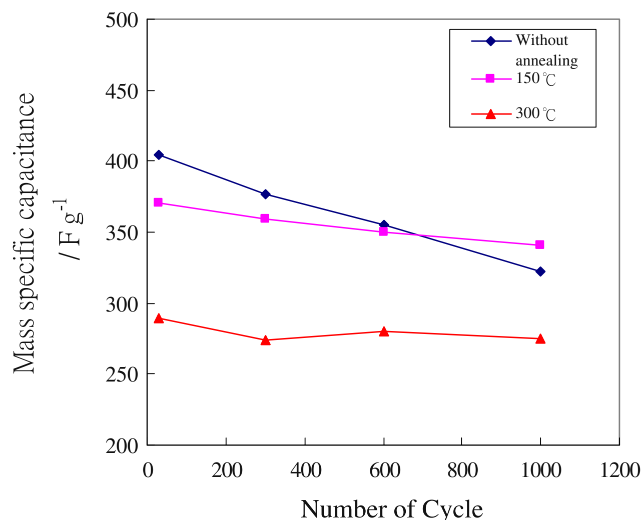

Fig. 9 The effects of different charge–discharge cycles and without annealing as well as with different annealing temperatures (150 and 300 °C) on the mass specific capacitance of the electrode (fabricated by optimum sputtering conditions: 5 sccm oxygen, 20 mTorr, and 70 W)

the highest mass specific capacitance value of 341 F g^{-1}. In addition, at the 30th cycle of potential cycling, the mass specific capacitance of the electrode without annealing was maximum due to its highest surface roughness and the mass specific capacitance of the electrode decreased with increasing annealing temperature since the higher the annealing temperature, the higher the kinetic energy, the higher the mobility on the surface of the substrate for particles and the lower the surface roughness (see Fig. 10). This picture also suggests that without annealing or at the lower annealing temperature, the manganese oxide with more porous structure (see Fig. 11) is more easily diffused into inner layers by the electrolyte ions (H^+: 76.7% and Li^+: 23.3% [40]), then some active sites on inner layers are able to contribute to mass specific capacitance, and thus

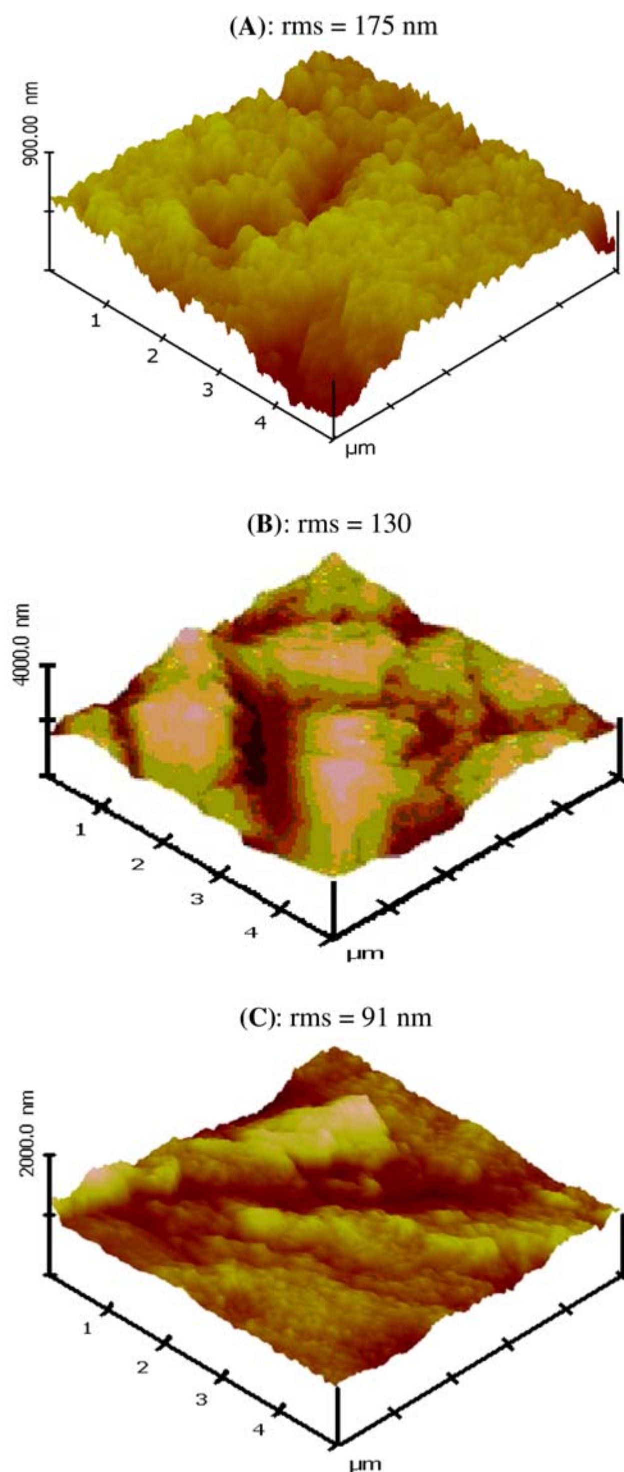

Fig. 10 AFM micrograph (**a** without annealing, **b** annealing temperature = 150 °C, and **c** annealing temperature = 300 °C) of the electrode (using optimum sputtering conditions: 5 sccm oxygen, 20 mTorr, and 70 W)

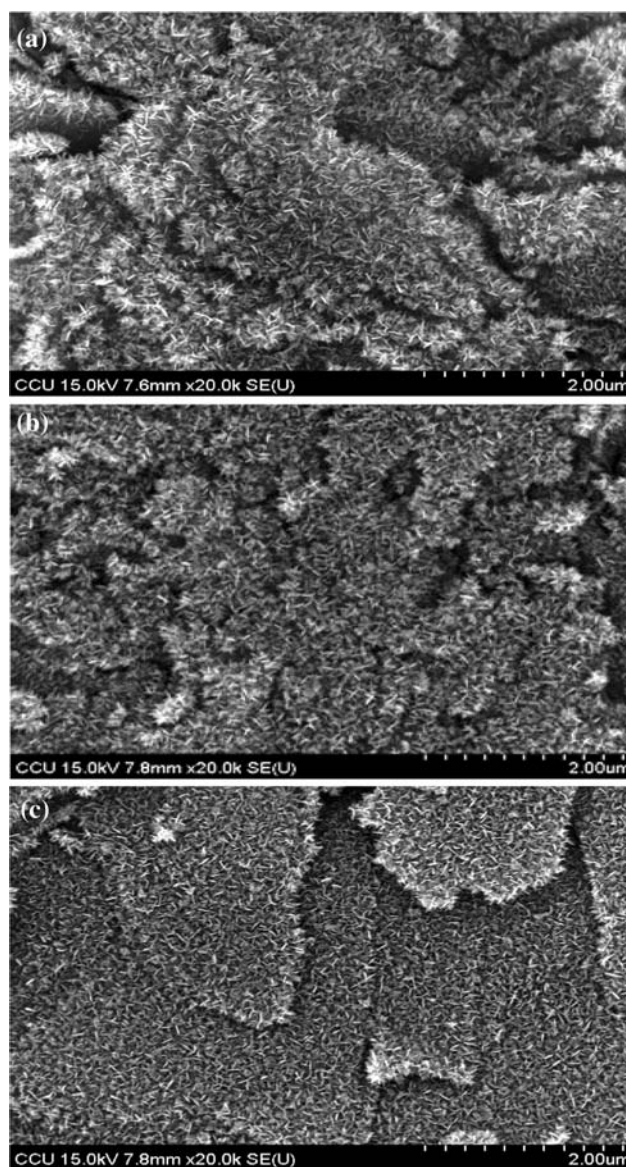

Fig. 11 SEM micrograph (**a** without annealing, **b** annealing temperature = 150 °C, and **c** annealing temperature = 300 °C) of the electrode (using optimum sputtering conditions: 5 sccm oxygen, 20 mTorr, and 70 W)

this leads to higher mass specific capacitance. Furthermore, the mass specific capacitance of the electrode without annealing decreased quickly with increasing number of charge–discharge cycles, but the mass specific capacitance of the electrode with annealing gradually decreased with increasing number of charge–discharge cycles and the higher the annealing temperature, the slower the decreasing rate of the mass specific capacitance. The reason behind this behavior may be that for the electrode without annealing, less compact than that of the electrode with annealing and the lower the annealing temperature, the less the compact (see Fig. 11), thus leading to more easily lose an irreversible mass (electrolyte color changed from transparent to turbid) by low dissolution and slow diffusion of active MnOOH (solubility about 10^{-5} mol l^{-1}) [41, 42].

4 Conclusion

A simpler one-step RF magnetron sputtering dry process was employed to deposit manganese oxide onto graphite foil and obtain maximum capacitance at optimum conditions. The mass specific capacitance increased at lower sputtering pressure/sputtering power, but decreased at higher sputtering pressure/sputtering power because of a shadowing effect/a too strong ion and reflected neutral bombardment. In addition, the mass specific capacitance of the electrode without annealing was maximum and decreased quickly with increasing number of charge–discharge cycles. However, the mass specific capacitance of the electrode with annealing gradually decreased with increasing number of charge–discharge cycles. Furthermore, the higher the annealing temperature, the lower the mass specific capacitance, but the slower the decreasing rate of the mass specific capacitance for charge–discharge cycles.

Acknowledgment Financial support by the National Science Council of the Republic of China (under grant no. NSC94-2622-E-224-022-CC3) is gratefully acknowledged.

References

1. Conway BE (1999) Electrochemical supercapacitors—scientific fundamentals and technological applications. Kluwer/Plenum, New York
2. Kotz R, Carlen M (2000) Electrochim Acta 45:2483
3. Chang JK, Tsai WT (2003) J Electrochem Soc 150:A1333
4. Chen YS, Hu CC (2003) Electrochem Solid-State Lett 6:A210
5. Jeong YU, Manthiram A (2002) J Electrochem Soc 149:A1419
6. Hu CC, Wang CC (2003) J Electrochem Soc 150:A1079
7. Park HP, Park OO, Shin KH et al (2002) Electrochem Solid-State Lett 5:H7
8. Reddy RN, Reddy RG (2003) J Power Sources 124:330
9. Broughton JN, Brett MJ (2004) Electrochim Acta 49:4439
10. Wu M, Snook GA, Chen GZ et al (2004) Electrochem Commun 6:499
11. Burke A (2000) J Power Sources 91:37
12. Chang JK, Lin CT, Tsai WT (2004) Electrochem Commun 6:666
13. Hong MS, Lee SH, Kim SW (2002) Electrochem Solid-State Lett 5:A227
14. Park JH, Ko JM, Park OO (2003) J Electrochem Soc 150:A864
15. Zhang JR, Chen B, Li WK et al (2002) Int J Mod Phys B 16:4479
16. Zheng JP, Jow TR (1995) J Electrochem Soc 142:L6
17. Zheng JP, Cygan PJ, Jow TR (1995) J Electrochem Soc 142:2699
18. Zheng JP (1999) Electrochem Solid-State Lett 2:359
19. Hu CC, Tsou TW (2002) Electrochim Acta 47:3523
20. Pang SC, Anderson MA, Thomas WC (2000) J Electrochem Soc 147:444
21. Lin CC, Yen CC (2008) J Appl Electrochem 38:1677
22. Lin CC, Chen HW (2009) Electrochim Acta 54:3073
23. Lim JH, Choi DJ, Kim HK, Cho WH, Yoon YS (2001) J Electrochem Soc 148:275
24. Ward LP, Datta PK (1995) Thin Solid Films 271:101
25. Koski K, Holsa J, Ernoult J, Rouzaud A (1996) Surf Coat Technol 80:195
26. Reiners G, Griepentrog M (1995) Surf Coat Technol 76–77:809
27. Liu H, Zhang X (1994) Thin Solid Films 240:97
28. Wang X, Yang G, Liu X, Zheng Z, Huang W, Zou S (1992) Mater Sci Eng A156:91
29. Ohring M (2002) Materials science of thin films. Academic Press, New York
30. Battaglin G, Rigato V, Zandolin S, Benedetti A, Ferro S, Nanni L, De Battisti A (2004) Chem Mater 16:946
31. Hu CC, Tsou TW (2003) J Power Sources 115:179
32. Huang JH, Chen JS (2001) Thin Solid Films 382:139
33. Chang JK, Chen YL, Tsai WT (2004) J Power Sources 135:344
34. Kim H, Popov BN (2003) J Electrochem Soc 150:D56
35. Lin CC, Yen CC (2007) J Appl Electrochem 37:813
36. Snook GA, Peng C, Fray DJ, Chen GZ (2007) Electrochem Commun 9:83
37. Lee HY, Goodenough JB (1999) J Solid State Chem 144:220
38. Toupin M, Brousse T, Bélanger D (2004) Chem Mater 16:3184
39. Chigane M, Ishikawa M (2000) J Electrochem Soc 147:2246
40. Kuo SL, Wu NL (2006) J Electrochem Soc 153:A1317
41. Wu BL, Lincot D, Vedel J, Yu LT (1997) J Electroanal Chem 420:159
42. Pang SC, Anderson MA (2000) J Mater Res 15(10):2096